Tellus (1993), 45B, 426–441
Printed in Belgium – all rights reserved

TELLUS
ISSN 0280–6509

A modeling study of the long-range transport of Kosa using particle trajectory methods

By VEERABHADRA R. KOTAMARTHI[1] and GREGORY R. CARMICHAEL[2], *Department of Chemical and Biochemical Engineering, University of Iowa 125B Chemistry Building, Iowa City, IA 52242-1219, USA*

(Manuscript received 1 December 1992; in final form 28 April 1993)

ABSTRACT

The long-range transport of dust in east Asia is analyzed using a conditioned-particle approach. A one-dimensional K–E model with algebraic stress is used to describe the boundary layer dynamics at various locations along the transport path. The turbulent flow fields created using the boundary layer model are used to simulate the transport and dispersion of dust during a spring storm in China. The particle movement studies in the resultant fields indicate that the turbulence is effective in dispersing the plume in the initial few hours after the emissions take place. The boundary layer shear starts dominating the plume dispersion at later times. The calculated plume growth rate is greater while traveling over land surface than when over the sea. This results from the greater strength of the diurnal oscillation and the larger boundary layer shear over the land surface compared to the sea. Calculated plume widths and concentrations are in good agreement with the limited available observations.

1. Introduction

Presently there is an increased awareness of the environmental problems associated with long-range transport (LRT) of pollutants. The LRT of pollutants is actively being studied in North America and Western Europe. Because these areas have been the center of the industrial activity they were the first to face the problems associated with the LRT of pollutants. With increasing industrial activity in other parts of the world, it is essential that the assessment of the effects of LRT on these newly industrialized regions come into focus. A region of particular interest at present is the Western Pacific Rim. This is one of the fastest economically developing regions of the world and the emissions from this region are expected to double in the near future (Hameed and Dignon, 1988).

Several studies (Kondo et al., 1987; Kotamarthi and Carmichael, 1990) have shown the potential for long-range transport of atmospheric pollutants in this region. The complex arrangement of land and sea surfaces along the transport path of a species in this region leads to interesting effects on their transport scales and life times. During the spring months the LRT in this region is usually associated with the dust storms in the Chinese deserts and Loesses plains. Several studies have been conducted to understand the transport paths of the so called "Kosa" (yellow sand) events in Japan (Iwasaka et al., 1983; Suzuki and Tsungai, 1988; Kai et al., 1988). Using back-trajectory calculations, the dust particles from this region were shown to be transported as far as the Hawaiian Islands (Merrill et al., 1985). The overall loading of dust particles from this region in to the Pacific Ocean is estimated to be larger than from the Saharan region of west Africa into the Atlantic Ocean (GESAMP, 1989). But the dust transport from this region and its consequences on the regional environment have received less attention than that given to Saharan desert. Prospero and

[1] Current Address: AER Inc., 840 Memorial Drive, Cambridge, MA, 02139, USA.
[2] Corresponding author.

Savoie (1989) have shown that particulate nitrate concentrations in the northern Pacific increase during Asian dust events and that most of the nitrate is of anthropogenic origin. In addition, these springtime dust transport episodes are often associated with periods of elevated tropospheric ozone. Thus there is a clear need to fully understand the physical and chemical processes controlling the trace gas cycles and aerosol dynamics in east Asia.

As a first step in studying the transport process, a methodology for analyzing the effects of boundary layer dynamics on dust transport on a regional scale was developed. Boundary layer meteorology is expected to play an important rôle in the disbursement of the dust from its source and its transport to a height of 2 km in the vertical direction and the subsequent long-range transport of the plume. The distribution of dust due to purely boundary layer phenomena and diurnal cycling is investigated in this paper. The occurrence of other local meteorological events like localized dust storms on one hand and the movement of large-scale pressure systems on the other, obviously enhances most of the transport processes considered here. But the effect of boundary layer dynamics on the distribution of the dust plumes on the scales considered here may be of primary importance in the over all transport processes (McNider et al., 1988).

The procedure described here uses a one dimensional K–E model to describe the atmospheric boundary layer, using inputs from analyzed meteorological fields, to provide the transport characteristics. The resulting detailed wind fields are then used to study the dust transport with the so called "conditioned particle technique" (Smith, 1968). In this paper the model is described and applied to study the "Kosa" transport. McNider et al. (1988) studied the long range transport of a plume, from a power plant in Australia, using a similar particle transport model with meteorological inputs derived from a boundary layer model. Their boundary layer model employed a prescribed eddy diffusivity profile. Yamada and Bunker (1988) also used the particle transport method to explore the movement of an inert tracer in a mountain valley flow system. Suzuki and Tsungai (1988) studied the transport of dust in the middle troposphere, from central China, using a particle transport model and with meteorological data obtained from a weather forecast model.

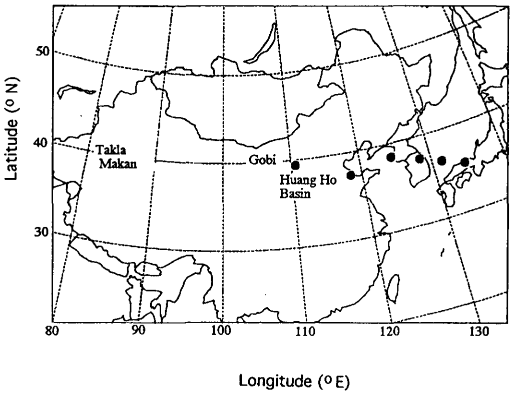

Fig. 1. Locations of source regions for Asian dust. The black dots are points where one dimensional simulations were performed using the meteorological model.

For comparison with the model simulations, a "Kosa" episode during the period 11th to 16th of April 1979 was selected. This event was studied using Lidar from Nagoya (long 137° E, lat 35° N) in Japan by Iwasaka et al. (1983). A dust plume was reported over Nagoya from the night of 14th to 16th of April 1979. Based on back trajectory calculations using the observed meteorological data, Iwasaka et al. (1983) have shown that the plume had its origin in China. The Lidar soundings showed that there were two dust clouds over Nagoya during this period. One at a height of approximately 2 km and the other at a height of 6 km. The 6 km cloud had its origin in Takla Makan and the 2 km cloud originated in Huong Ho basin in Northern China (Fig. 1). The 2 km level cloud in principle could be influenced extensively by the boundary layer meteorology and was chosen for this study for demonstrating this modeling methodology.

2. Modeling methodology

The primary motive of the study is to investigate the regional scale transport of inert dust under the influence of boundary layer dynamics. Particle transport calculations were performed on a regional scale in this study. The following methodology was adopted to represent the nonhomogeneous character of the terrain and its effect on the meteorology. An area of importance for the particle transport was selected, then, at several carefully chosen points in this domain a number of one dimensional simulations using an atmospheric boundary layer model were performed. The points were chosen to reflect the essential non-homogeneous characteristics of the region. The results from the model simulations were mapped over the domain of interest by interpolation to obtain a 80 km × 80 km distribution of the meteorological data in the horizontal plane. In the vertical direction data was obtained at every 5 m in the lowest 70 m of the domain. For the reminder of the domain extending to a height of 3000 m a logarithmic scale with 25 additional grid points was used. The movement of particles in this newly created meteorological field was studied using the conditioned particle technique (Smith, 1968). Each of these steps is explained in greater detail below.

2.1. *Particle transport calculations*

Particle trajectories are calculated using the so-called conditioned particle technique (Smith, 1968). This method was employed to study the transport of plumes by McNider et al. (1988) and to study transport of inert tracers by Yamada and Bunker (1988). Similar simulations, though on a smaller scale, were performed by Reid (1979), Ley (1982) and Thomson (1984). Their simulations yielded satisfactory results when compared to analytic solutions and experimental data. This is a particularly useful tool for the present study, as we are investigating the movement of inert dust plumes in the boundary layer over long distances.

The particle locations are computed using the expression

$$X_i(t+\Delta t) = X_i(t) + U_{pi}\,\Delta t, \tag{1}$$

where X_i is the particle location in the i direction ($X_1 = x$, $X_2 = y$ and $X_3 = z$), Δt is the time increment and U_{pi} the Lagrangian velocity of the particle prescribed as

$$U_{pi} = U_i + u_i. \tag{2}$$

U_i is the mean wind velocity in the i direction ($U_1 = U$, $U_2 = V$ and $U_3 = W$) and u_i ($u_1 = u$, $u_2 = v$ and $u_3 = w$) is the fluctuating component of the non buoyant particle velocity in a turbulent field. The fluctuating component of the velocity is represented as

$$u_i(t+\Delta t) = a u_i(t) + \sigma_{ui}(1-a^2)^{1/2}\,\lambda + \delta_{i3}(1-a)\,T_{li}\frac{\partial \sigma_{ui}^2}{\partial z}, \tag{3}$$

where

$$a = \exp(-\Delta t/T_{li}) \tag{4}$$

and the last term on the right hand side is that recommended by Legg and Raupach (1982) to prevent the movement of the particles towards regions of low turbulence. The auto correlogram was assumed to be of exponential form in the above set of equations and λ, a random number, chosen from a distribution with zero mean and a standard deviation of 1. The rms deviations of the fluctuating component of the velocity σ_{ui} and the mean velocity U_i have to be determined from a meteorological model.

The parameters in the above model not determined from the meteorological model namely, the Lagrangian time scales, T_{lx}, T_{ly} and T_{lz}, are set as follows. The Lagrangian time scales in the horizontal plane were set equal to the inverse of the Coriolis parameter as suggested by Gifford's (1982) analysis. This should provide a satisfactory estimate for the range of transport scales considered here. However setting the Lagrangian time scale in the vertical direction is much more difficult and there are several available estimates for different stability conditions in the literature. The basic assumption is that $T_{lz}/T_{ez} = \beta$, where β is a constant and T_{ez} is known as the Eulerian time scale of the velocity correlation's. Several experimental results (Pasquill and Smith, 1983) suggest that the value of βi lies in the range of 0.3 to 0.8, where i is the intensity of turbulence and is defined as σ_u/U. We have employed a value of 0.8 for all conditions. T_{ez} is thus estimated as $0.2\mathrm{H}/\sigma_u$ (Hanna, 1981) were H is the depth of the atmospheric boundary layer. An upper limit of 600 was set on this estimate, which roughly corresponds to $\beta < 10$ (McNider et al., 1988). Several values of Δt were tested ranging from 2 to 30 s and a value of 10 s was found to satisfactorily describe the particle displacement.

3. Meteorological model

A one-dimensional numerical model was implemented to obtain the pertinent meteorological data required to perform the particle trajectory calculations. Models of varying complexity are described in the literature ranging from the constant eddy diffusivity model to third order closure schemes (Mellor and Yamada 1974). The eddy diffusivity models are efficiently implemented but require a large amount of empirical formalism. The higher order models are complex and difficult to implement numerically, specially in multi-dimensions.

A compromise approach is being adopted by many modelers at present. Instead of solving the transport equations for the Reynolds stress terms, as in a second order closure model, several approximations are made to obtain algebraic expressions for the Reynolds stress terms. This process yields expressions for eddy diffusion coefficients in a form similar to the Kolmogorov–Prandtl expression (eq. (10)). Unlike the Kolmogorov–Prandtl expression the coefficient in eq. (10) is a function of the stability. Thus the K–E model formulation usually involves solving the equations for U, V, Θ and additional ones for kinetic energy and dissipation rate. Here U is the mean velocity in the x direction, V the mean velocity of the air in the y direction and Θ is the mean potential temperature. Equations for modeling the dissipation rate were proposed by Rodi (1976), in a form similar to the one discussed here. This type of model was used recently by Uno et al. (1989), to simulate the nocturnal boundary layer in an urban environment. The fundamental aspects of the model are discussed in detail by Rodi (1985) and Uno and Ueda (1988). We have adopted this so called K–E model with the algebraic stress component for the present study.

The relevant equations for the one-dimensional meteorological model after making the Boussinesq approximation can be written as:

U-momentum equation:

$$\frac{\partial U}{\partial t}=\frac{\partial(K_m(\partial U/\partial z))}{\partial z}+f_c(V-V_g) \tag{5}$$

V-momentum equation:

$$\frac{\partial V}{\partial t}=\frac{\partial(K_m(\partial V/\partial z))}{\partial z}-f_c(U-U_g). \tag{6}$$

Heat balance equation:

$$\frac{\partial \Theta}{\partial t}=\frac{\partial(K_h(\partial \Theta/\partial z))}{\partial z}+\text{rad}. \tag{7}$$

Kinetic energy balance equation:

$$\frac{\partial K}{\partial z}=\frac{\partial(K_m(\partial K/\sigma_k\,\partial z))}{\partial z}+P+G-E. \tag{8}$$

Dissipation equation:

$$\frac{\partial E}{\partial t}=\frac{\partial(K_m(\partial E/\sigma_e\,\partial z))}{\partial z}+\frac{C_{1E}}{K}(P+(1-C_{3E})\,G)$$
$$-C_{2E}\frac{E^2}{K}, \tag{9}$$

where P is the shear production term of turbulent kinetic energy defined as $-\langle uw\rangle\,\partial U/\partial z$, G is the buoyancy production term of turbulent kinetic energy and is defined as $g/T\langle w\theta\rangle$, U_g and V_g are the geostrophic components derived from temperature variations along the horizontal axis, and f_c is the Coriolis parameter. K_m and K_h are the eddy mixing coefficients which are modeled according to the algebraic stress model (Rodi, 1985) as

$$K_m=C_\mu\frac{K^2}{E}, \tag{10}$$

with

$$C_\mu=-\omega\frac{\langle w^2\rangle}{K}, \tag{11}$$

and u, w and θ are the fluctuations from the mean fields. The mean vertical wind component W is zero for the one dimensional model. The curved brackets indicate an ensemble mean average of the fluctuating quantities.

The algebraic stress model (ASM) represents this ensemble mean as (Uno et al., 1989):

$$\frac{\langle w^2\rangle}{K}=\frac{2(C_1-1+P/E(C_2-2C_2C_{2w}f)+G/E(3-2C_3))}{3(C_1+2C_{1w}f+(P+G/E)-1)}. \tag{12}$$

Similar equations can be derived for the other set of second-order turbulence statistics (Rodi, 1985). The constants C_1, C_2, C_3, C_{2w} and C_{1w} are provided in Table 1 and are the same as those used by Uno et al. (1989). These constants are obtained from the pressure correlation model as discussed by Gibson and Launder (1978). The variable f is known as the wall proximity function and is defined following Uno et al. (1989) as

$$f=\left(\frac{\lambda}{\kappa z}\right)^2, \tag{13}$$

and λ is defined as

$$\lambda=C_{\mathrm{L}}\frac{\langle -uw\rangle^{3/2}}{E}, \tag{14}$$

with $C_{\mathrm{L}}=0.18$, a constant.

The parameter ω is a function of stability parameters and is defined by the following set of equations following Rodi (1985) and Uno et al. (1989):

$$\omega=\frac{1-C_2+\frac{3}{2}C_2C_{2w}f-A(1-C_3)(1-C_{2t})\,\alpha B}{A_1+A(1-C_3)\,B} \tag{15}$$

$$\alpha=\frac{A_2}{1+2A_2RB(1-C_{3t})}, \tag{16}$$

$$B=\frac{\beta g K^2}{E}\frac{\partial\Theta}{\partial z}, \tag{17}$$

$$A_2=1.0\bigg/\left(C_{1t}+C_{1tw}f+0.5\left(\frac{P+G}{E}-1\right)\right), \tag{18}$$

$$A_1=1.0\bigg/\left(C_{1t}+0.5\left(\frac{P+G}{E}-1\right)\right), \tag{19}$$

$$A=1.0\bigg/\left(C_1+1.5C_{1w}f+\frac{P+G}{E}-1\right). \tag{20}$$

The constants in these equations are as before obtained from the pressure correlation model and are presented in Table 1.

The eddy mixing coefficient for the temperature equation can be expressed in a similar fashion as

$$K_{\mathrm{h}}=C_{\mathrm{h}}\frac{K^2}{E},\qquad \text{where}\quad C_{\mathrm{h}}=-\alpha\frac{\langle w^2\rangle}{K}, \tag{21}$$

and with α as expressed above.

The radiative flux term (Rad) is calculated using the simplified scheme of Sasomori (1968). More details of this scheme can be obtained from Pielke (1984). An initially defined water vapor concentration is held constant throughout the computations for making the radiation calculations.

Table 1. *Numerical values of constants appearing in the ASM (Uno et al. (1989))*

C_1	C_2	C_3	C_{1w}	C_{2w}	C_{1t}	C_{2t}	C_{3t}	C_{1tw}	R
2.6	0.38	0.38	0.21	0.22	2.85	0.0	0.22	0.31	0.8

The remaining constants in the dissipation equation $C_{1\mathrm{E}}$, $C_{2\mathrm{E}}$ and $C_{3\mathrm{E}}$ are set to $C_{2\mathrm{E}}=1.92$, $C_{1\mathrm{E}}=1.44$ (Rodi, 1985; Stubly and Rooney, 1986; Kitada, 1987) and $C_{3\mathrm{E}}=0.0$ for stable conditions and 1.0 for unstable conditions. This was shown to be a good approximation for atmospheric situations by Duynkerke (1988). The Prandtl numbers σ_{k} and σ_{e} are set to a value of 1.0 and 1.3 (Rodi, 1985; Kitada, 1987).

3.1. Boundary conditions

The velocities are set equal to zero at the lower boundary. The ground surface temperature was computed using the force restore method of Bhumralkar (1971). Familiar forms of the Monin Obukhov similarity profile relationships are used to compute the fluxes at the lowest grid point of the computational domain (2.5 m). The equations used for computing the lower boundary conditions for the kinetic energy and dissipation are

$$K=C_{\mu 0}^{-1/2}u^{*3}, \tag{22}$$

$$E=\frac{u^{*2}}{kz}\left[\Phi_m-z/L\right]. \tag{23}$$

The Businger–Dyer flux relationships are used to define Φ_{m} and Φ_{h} (Pielke, 1984). A value of 2.0 was assigned to $C_{\mu 0}$ (Uno and Ueda, 1988). In the above equations, L is the Monin-Obukhov length scale in the surface layer (Pasquill and Smith, 1983), u^* is the frictional velocity at the surface of the earth and k is the von Karman constant. At the upper boundary the velocity gradients are set equal to zero and the potential temperature gradient is set to a value of 2 degrees 2°K/km.

3.2. Numerical procedure

A linear grid size of 5 m was used in the lowest 70 m of the domain changing to a non-linear scale to the top of the model domain. The top of the model domain was set at a height of 3000 m for all the computations. A total of 40 grid points were used. A fully implicit finite difference scheme was used (Richtmeyer and Morton, 1967). The velocities U, V were calculated at the edge of the grid volume and the remaining quantities were computed at the center of the grid. A time step of 5 s was used for all computations. The simulations were initially started using an eddy diffusivity model with an eddy diffusivity profile described according to O'Brien (1970). After half an hour of computation the calculations were switched over to the present model.

Thus the model is capable of producing mean wind fields and turbulence statistics in one dimension using initial velocity, temperature, surface conditions and geostrophic wind velocities as inputs.

3.3. *Model verification*

A test run was made for day 33 of the Wangara data set (Yamada and Mellor, 1975; Andre et al., 1978; Sun and Chang, 1986; Pielke and Mehrer, 1975) to validate the boundary layer model. The initial and boundary conditions were also set as described in Yamada and Mellor (1975). The geostrophic wind components were set according to their procedure. The model calculations were performed to a height of 2 km for the test case using a total of 35 grid points.

Fig. 2 shows the calculated U wind component along with the observed wind for 12 noon. This shows the development of a well mixed boundary layer in the morning hours. Also plotted are the calculated results from Sun and Chang (1986). Sun and Chang used an eddy diffusivity model where the eddy diffusivity coefficients are related to the kinetic energy by an equation of the type $K_m =$ const. $\lambda K^{1/2}$, where λ, a turbulent length scale, is estimated from an empirical correlation. The model results compare favorably with the results of Sun and Chang (1986) and to the observed values. The differences between the model predictions above the boundary layer may be due to the different geostrophic wind velocities employed. The calculated values are also presented for 3 am in the morning. This compares favorably to the profile calculated by Yamada and Mellor (1975) using a more sophisticated model. The model calculated values of a parameter of more interest here σ_w is presented in Fig. 3 at 14:00 hrs. These results compares favorably with those calculated by Deardorff (1974) using a boundary layer model with a second order closure scheme. The maximum values are reached somewhere in the middle of the boundary layer and then start decreasing slowly.

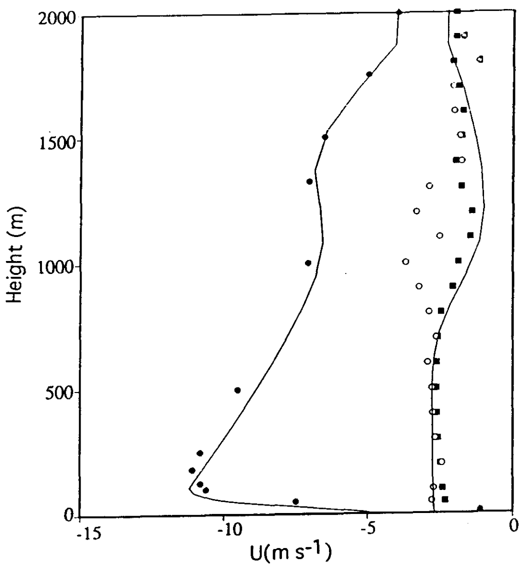

Fig. 2. Meteorological model predictions of U-velocity component. Left-hand curve represents profile at 12:00 local time and the right hand curve at 3:00 local time. (○) represents measured values, (■) predictions of Sun and Chang (1986) and (●) predictions of Yamada and Mellor (1975).

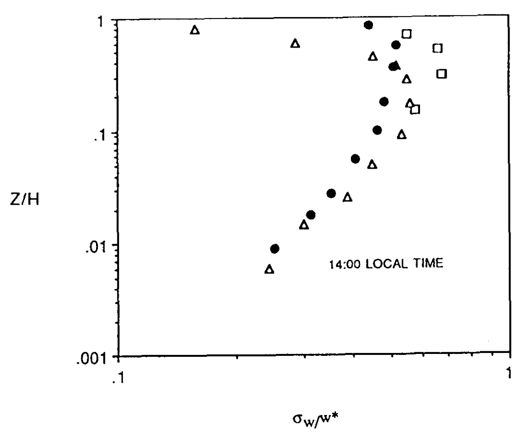

Fig. 3. Predictions of σ_w/w^* by the meteorological model (●) for Wangara day 33 compared with the predictions of (□) Deardorff (1974), (△) McNider et al. (1988).

4. Meteorological inputs for particle trajectory calculations

The three-dimensional meteorological fields necessary for the particle trajectory calculations were constructed based on several sets of runs with the one dimensional meteorological model at selected locations in the domain of interest. The domain of interest stretches from 109.5° E to 137.5° E longitude and 30.5° N to 40.5° N latitude. The domain was divided into grid cells of 1° longitude by 1° latitude for making the particle calculations. A total of 6 points where chosen in this domain to make the one dimensional meteorological calculations. The locations of the points are shown in Fig. 1. The various locations are differentiated in that they were assigned different surface roughness parameters according to their location. In addition the points over the sea surface was assigned a constant surface temperature of 285.0°K for the entire simulation period. This gives a slightly unstable condition at the sea surface for the entire simulation time, the temperature difference between the sea surface and the lowest grid point above it (2.5 m) being 2°C at the most. All the points over land were assigned a surface roughness value of 1 cm (to represent grass surface and sparse vegetation), except for one point, located near the source region, which was assigned a value of $6.0 \cdot 10^{-2}$ to simulate desert conditions. The surface roughness value over the sea surface was prescribed as

$$z_0 = 0.032 u_*^2 / g, \tag{24}$$

with the restriction that $z_0 \geqslant 0.0015$ cm (Clarke, 1970).

The initial conditions and geostrophic winds were derived from a data set of observed soundings obtained for this region from NCAR (National Center for Atmospheric Research) for April 1979. The data sets chosen for analysis are 11/15 of April 1979, to study the dust storm event discussed before. A total of 50 observations were noted for this region for that particular period for an area slightly bigger than the selected domain for each of 12-h intervals. Wind fields were developed for this region using linear interpolation in the vertical and a horizontal interpolation using $1/r^2$ as the weighting factor on to a grid of 1° × 1°. This wind field was adjusted for divergence using the procedure suggested by Goodin et al. (1978). The geostrophic wind components required for the one-dimensional simulations at 0, 1, 2, 3 km were obtained using the temperature data and the surface pressure values derived from this data set. A single average value of the geostrophic components was used for the entire modeled layer. The geostrophic wind direction obtained was westerly for all the data points. The geostrophic wind velocities used for simulation at one of the location are presented in Table 2. The soil parameters were set to representative values indicated by Deardorff (1978).

Table 2. *Geostrophic wind velocities and shears used at 38.5° N and 110.5° E*

Date	Time	Geostrophic wind velocity (m s^{-1})	Geostrophic shear (s^{-1})
11 April 1979	12 GMT	2.00	0.004
12 April 1979	00 GMT	2.00	0.006
12 April 1979	12 GMT	3.75	0.006
13 April 1979	00 GMT	6.26	0.006
13 April 1979	12 GMT	2.67	0.005
14 April 1979	00 GMT	7.41	0.005
14 April 1979	12 GMT	2.00	0.005
15 April 1979	00 GMT	2.00	0.006

Fig. 4 shows the calculated $\langle w^2 \rangle$ contours for a single day at long 110.5° E and lat 39.5° N. The profiles show the expected behavior with a maximum somewhere near the lower 500 m from the surface and its value decreasing towards the top of the ABL. The maximum values were obtained at about 14:00 LT as expected. Fig. 5 shows the

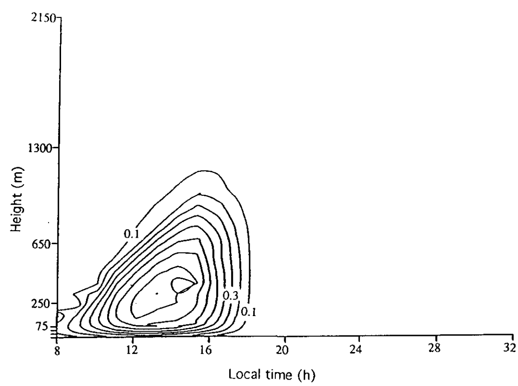

Fig. 4. Predictions of $\langle w^2 \rangle$ contours for a 1-day period (long 110.5° E and 39.5° N).

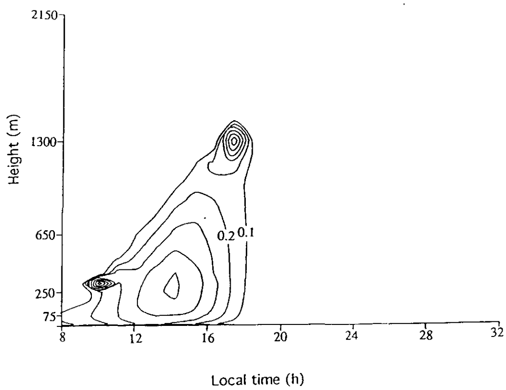

Fig. 5. Predictions of $\langle u^2 \rangle$ contours for a 1-day period (same location as Fig. 4).

calculated $\langle u^2 \rangle$. The value of $\langle u^2 \rangle$ reaches a maximum value very near the top of the boundary layer during the local sun set, where as during the mid-afternoon period it is below 500 m. Fig. 6 shows the calculated profiles of $\langle w^2 \rangle$ for a point over sea (long 124.5°E and lat 38.5°N). The computed values over the sea were less than the land values and the boundary layer is shallow compared to land surface.

The domain chosen for this study includes a single dust source area located at the edge of the Huong Ho basin area shown in Fig. 1. This was shown to provide the 2 km level dust cloud by Iwasaka et al. (1983) for the April 1979 dust event. The results of the one-dimensional simulations performed for a four day period with varying geostrophic winds to represent in a sense the varying synoptic scale forcing during this period were mapped on to this domain using the same procedure as described before for the observed winds (1° × 1° resolution). The interpolations for the rms deviations were performed such that only land surface values were used for interpolations over land and the sea surface values used for generating values for the grid points over the sea. The resulting plot for $\langle w^2 \rangle$ in a slice along the $x-z$ plane is shown in Fig. 7, at 14:00 local time. This shows that the present method gives a non-homogeneous distribution of turbulence statistics in the domain of study. The differences in the values of $\langle w^2 \rangle$ over different land surface points are mostly due to differences in the surface roughness and the geostrophic forcing employed in the study.

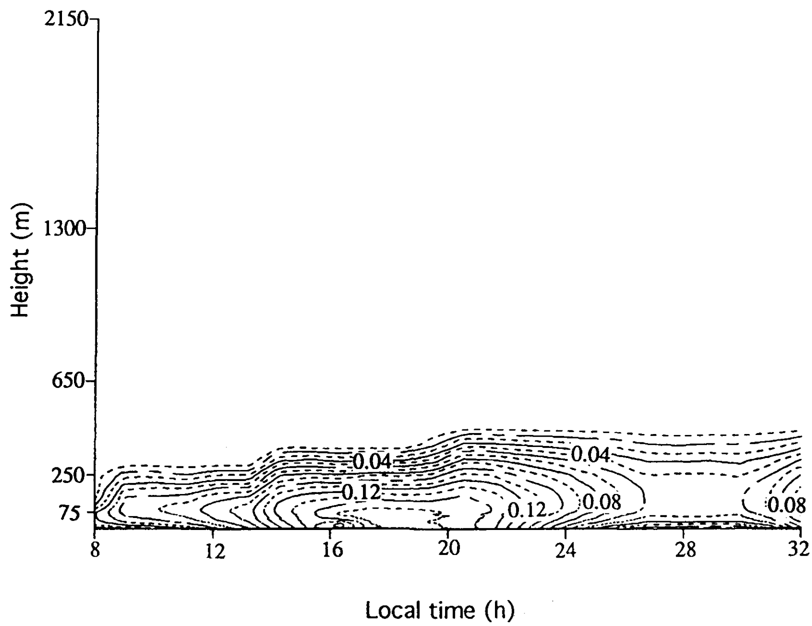

Fig. 6. Predictions of $\langle w^2 \rangle$ contours for a 1-day period over sea (long 124.5°E, 37.5°N).

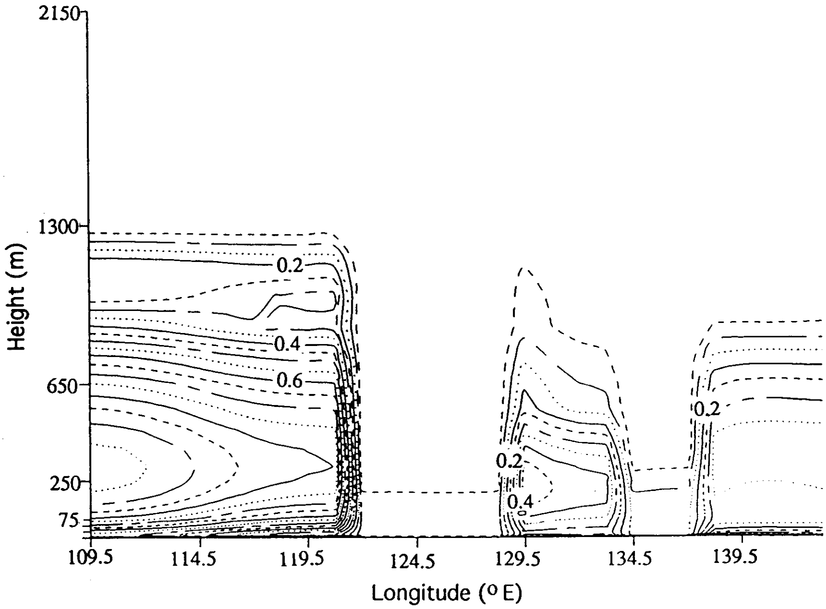

Fig. 7. Interpolated values of $\langle w^2 \rangle$ in space along a vertical cross section at 14:00 local time.

5. Three-dimensional particle release studies

Two types of particle release techniques were employed. In the first set, all the particles were released at the same moment and their random components set separately. We will refer to this as a puff release. In the second case a continuous stream of particles was released over a 4-day period at the rate of one particle per minute, giving a total of 5760 particles. This is referred to as the continuous release case. All the particles were released approximately at 10°N longitude 35°E latitude corresponding to the edge of the Huang Ho basin. The meteorological data was updated at the end of every one hour of simulation for performing the particle trajectory calculations. Since the interpolated data is available only at intervals of 1° longitude and 1° latitude, the meteorological variables for particles located at points inside the grid cells were calculated using the data from the nearest 8 neighboring grid points. The ground surface was assumed to be elastic for particles impinging on it.

5.1. Puff release

The particles were initially released instantaneously at 110°N and 35°E at 12 GMT of 11 April 1979 (Case 1). This corresponds approximately to 8 am local time (LT) on the morning of 12 April. Fig. 8 shows the position of particles after 90 h of travel for a puff release. It clearly shows that the particles spread out by nearly two degrees in the cross wind direction and more than 10° in the longitudinal direction. This gives a total area coverage of about 1.0E + 06 km^2 in the horizontal direction. This compares favorably with

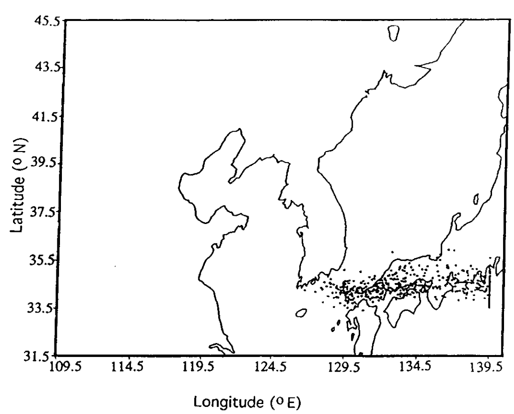

Fig. 8. Particle locations as a result of instantaneous release of particles after 96 h of diffusion time.

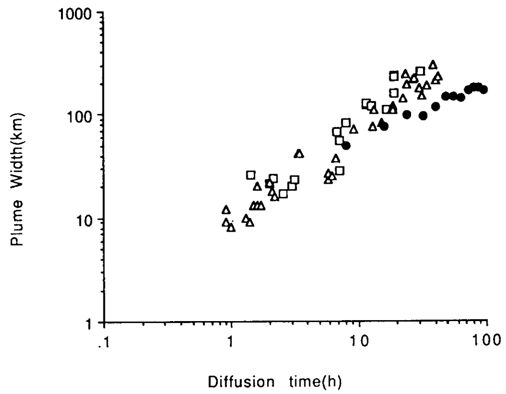

Fig. 9. Plume width (km) for puff release. (□) data of Bigg et al. (1978), (△) Carras and Williams (1981), (●) present simulation.

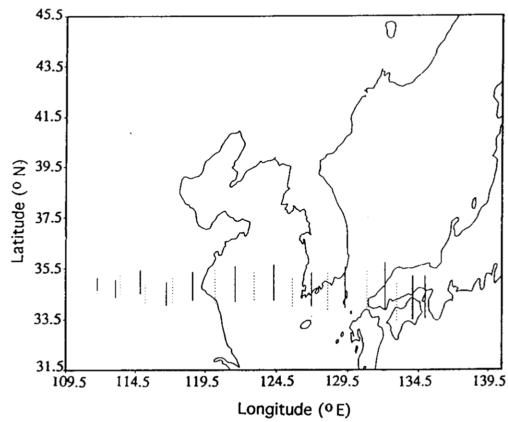

Fig. 10. Plume widths at various horizontal distances along the path of plume travel. Dotted line represents particles released 8 h after the release of particles represented by the continuous line.

the estimate of Iwasaka et al. (1983) of the average plume area as 1.36E + 06 km^2 as determined from satellite photographs and other means. They also reported that dust was observed in the Nagoya area approximately from the night of 14–16 April 1979. The simulation results show that the dust plume is well over Nagoya at the end of nearly four days of travels as shown in the figure, corresponding to these reported times.

One interesting quantity that can be compared with other long range transport observations is the cross wind spread of the plume. The cross wind spread was calculated as 4.28 × the standard deviation of all the particle positions from their mean position. This corresponds to a 90% concentration cut off. Fig. 9 shows the cross wind spread of the plume compared with the observations of Carras and Williams (1981) and Bigg et al. (1978) from a power plant in Australia, for various diffusion times. The predictions are in close agreement for the initial times. But as time progresses the predictions start falling below the experimental values, and at times greater than 50 h the plume growth has slowed down considerably. These and other effects of the non homogeneous nature of the meteorological inputs used to make the particle transport calculations are discussed below.

5.2. *Effects of non-homogeneity*

Several interesting features can be noted from Fig. 9. The plume grows rapidly in the first 24 h of diffusion, and after a no-growth period of 8 h, it again starts growing rapidly in the early evening hours and throughout the night for the next 16 h. But after 48 h, even though a similar cycle is evident, the effects are very diminished. Besides the plume does not grow appreciably while traveling over the sea as is evident from Fig. 10.

One reason for the plume growth being stationary over the sea surface could be related to the start time of the particle calculations. It may be that the plume reached the sea surface during the day time non-growth period. To test this hypothesis a set of simulations were performed by releasing the particles 8 h later than the previous experiment (16.00 hrs local time, Case 2). Fig. 10 shows the resulting plume spreads, represented by the dotted lines. It can be seen that there is no apparent increase in plume width over the sea surface due to this. Also the overall plume width was smaller than obtained from the previous experiment. Thus the release time appears not to be the critical factor in describing the observed effects.

Another important factor could be the decreased turbulence over the sea surface. To test the effect of the turbulence a new set of turbulence data was used, generated by assuming the entire study region was composed of land surface. This could be expected to give a more homogeneous turbulence structure over the domain. Again particles were released in this field at 8:00 a.m. local time at the same location as Case 3. The results of this experiment are shown in Fig. 11. The gain in

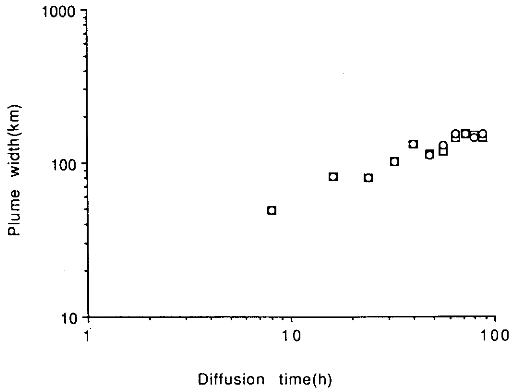

Fig. 11. Plume widths for puff release (○) with non homogeneous turbulence statistics and (□) with homogeneous turbulence statistics.

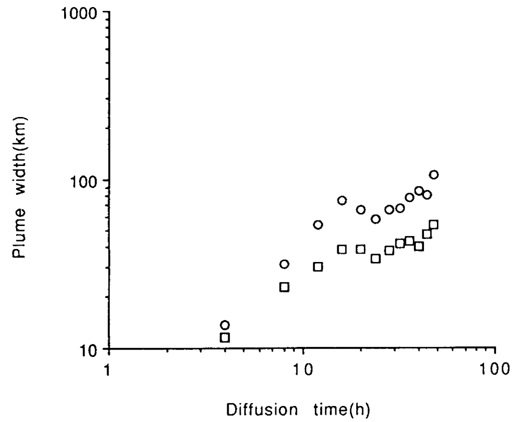

Fig. 12. Plume widths of particles released at about 100 km inland from the sea. (□) with non homogeneous turbulence and (○) with homogeneous turbulence.

plume growth as a result of this modification is minimal. This result is anticipated since it is unlikely that turbulence can play a significant part in plume growth after such long diffusion times.

To test the growth behavior of plumes over the sea surface several additional sets of numerical tests were performed. Particles were released instantaneously at a location close to the sea (100 km inland from the sea) keeping the release time the same as in Case 1 (Case 4). The turbulence fields were non homogeneous in the sense described before. The particles were followed for a period of 48 h. The particles under these conditions reach the sea surface after less than 8 h of travel time as compared to nearly 48 h for Case 1. The plume widths obtained (Fig. 12) are vastly reduced, and are only about 37% of those for the first 48 h in Case 1 simulation. The mean horizontal movement of the plume in this experiment was much slower than the for Case 1. The plume in Case 1 traveled 1.5× faster than this plume. If we compare the plume widths after the particles have traveled for the same distance in both the cases (500 km), this plume was about 48% of the land based plume.

Repeating this comparison, but now using the homogeneous turbulence fields (Case 5) in the sense described before we get a plume that is 71% of the plume observed in Case 1. The plume in Case 1 is now 1.13× faster than Case 5. Fig. 12 shows the comparisons of plume growths obtained from the last 2 experiments. There is little growth after the first 16 h of travel.

The reason for the above behavior could be the differences in geostrophic shears used at different points over the domain. On average, the geostrophic shear over land has a value of 0.0041 whereas over the sea it has a value of 0.0034. Another interesting factor can be seen from Fig. 13. It shows the trajectory of a particle released in the mean wind field without any turbulence at about 600 m from the ground level. The release time is unchanged from that used in Case 1. It shows that the strong curving observed on the first day has decreased on the second day and that during the time it is traveling over the sea surface it is almost straight. This could be due to different

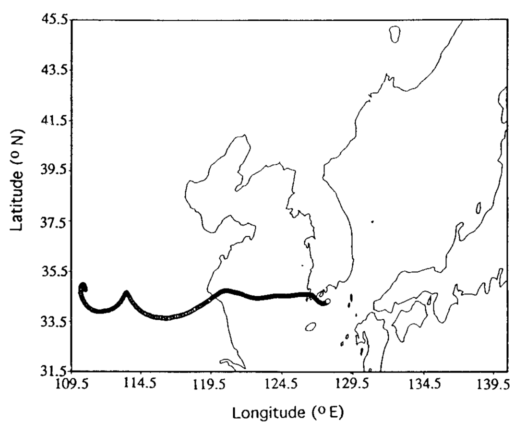

Fig. 13. Path traced by particles moving with the mean wind field without any turbulence.

geostrophic shears employed and the absence of strong ABL shear over the sea surface during the early evening hours due to a boundary layer that is almost stationary during the entire process. Thus it seems reasonable to assume that the geostrophic forcing and the ABL shear are the major factors affecting the growth and the absence of it at later times in the present numerical simulations.

5.3. Continuous release

In the next set of numerical experiments the particles were released as a continuous stream, at the rate of one particle every minute starting at 12 GMT on the 11 April. Fig. 14 shows the spread of particles released as a continuous stream, at the end of a 4-day simulation, across the domain. The shearing of particles along the wind is very apparent in this figure. Also the effect of the

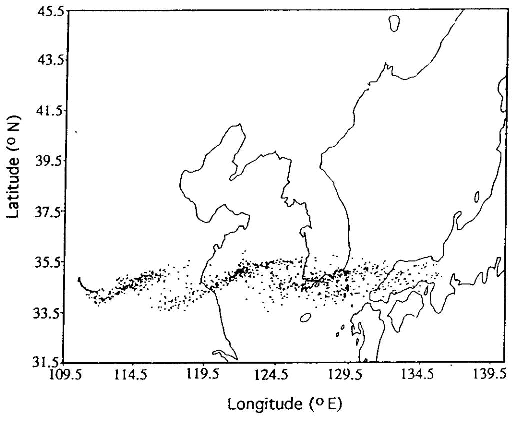

Fig. 14. Particle locations in space for a continuous release at the rate 1 particle per minute after 96 h of diffusion time.

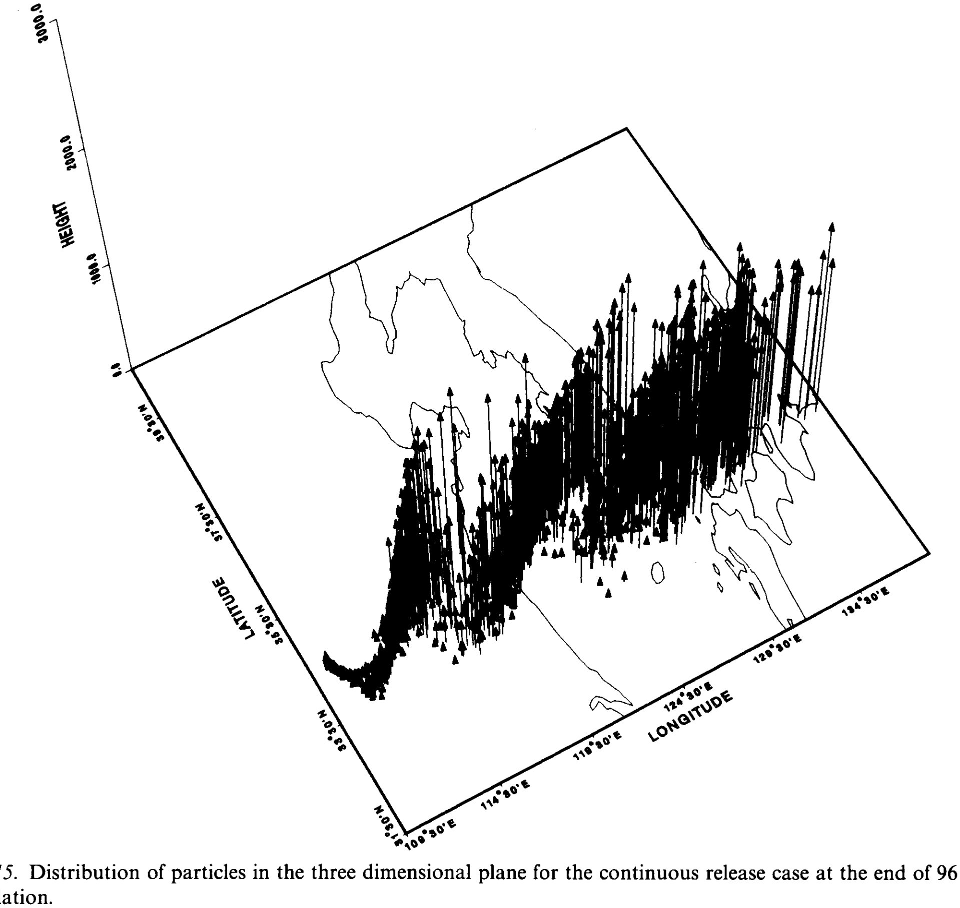

Fig. 15. Distribution of particles in the three dimensional plane for the continuous release case at the end of 96 h of simulation.

Coriolis force is evident in the meandering of the plume giving the so called "hose effect". It is also interesting to see the effect of turbulence on the spreading of the particles. From the experiments with turbulence over sea (Case 4) it is apparent the effect of turbulence is mainly at initial times where it plays a very important role in raising and mixing the particles in the vertical direction. The subsequent mixing and spreading of the plume is mostly due to the effect of wind shear. Fig. 15 shows the distribution in the three-dimensional plane of the same particle population as discussed before. After rising to a certain height about (600 m mean) the particles tend to maintain their height distributions throughout the travel, though showing considerable variations in day and night on the short term. The particles that were released at ground level are quickly mixed in the vertical direction as can be seen from this figure. Not many particles raise above the boundary layer height which is approximately 1500 m over the land surface. This may be an important factor that may not hold in real situations where local circulation's can lift the plume to higher levels than predicted by the present analysis.

The horizontal spread of the plume as a function of downwind distance is shown in Fig. 16. Plume widths for a continuous source were calculated using a 40-km wide area along the x-axis and all the particles in it were used for computing the plume width. These results are in good agreement with the observational data until about 1000 km during which time the particles are over the land. Beyond this distance there are considerable variations as a result of effects described earlier.

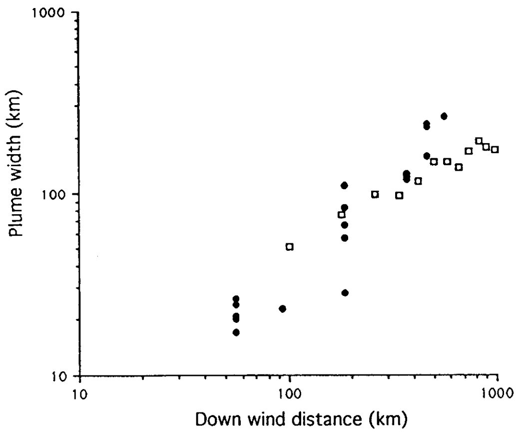

Fig. 16. Plume widths obtained for continuous release of particles (56 h from the start of simulation). (●) data of Carras and Williams (1981) and (□) results from the present simulation.

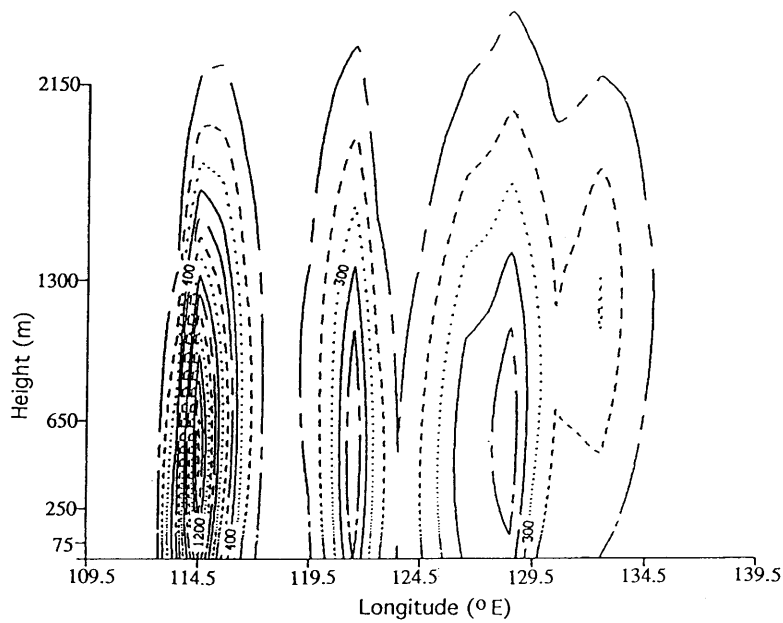

Fig. 17. Concentration contours for continuous release of particles ($\mu g/m^3$).

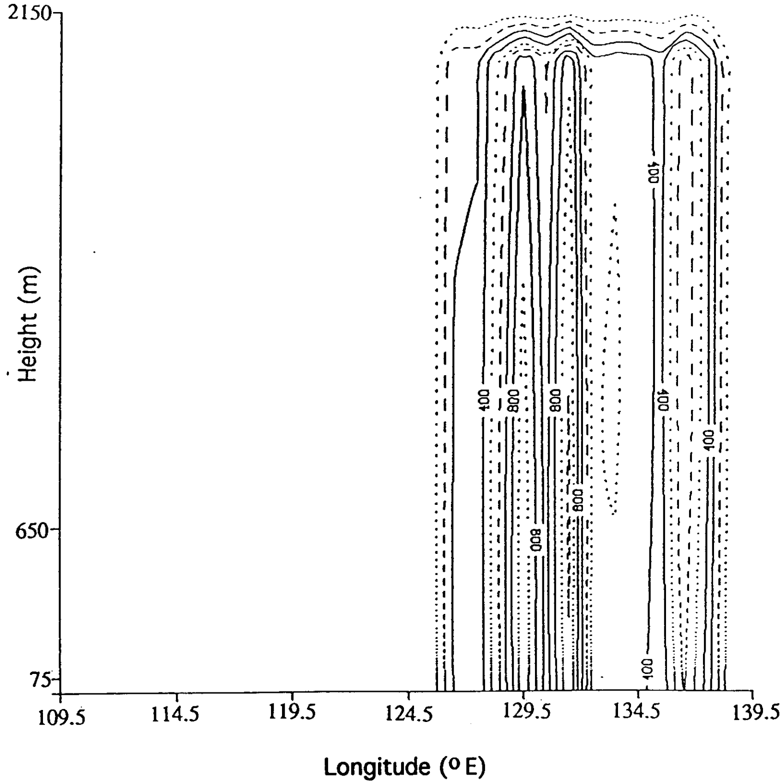

Fig. 18. Concentration contours for puff release of particles ($\mu g/m^3$).

5.4. *Concentration estimation*

Fig. 17 shows the concentration profiles estimated using a Gaussian kernel density estimator (Yamada and Bunker, 1988). This method was shown to require fewer numbers of particles than the traditional particle in cell methods and give satisfactory results. There were no limits set on the band widths allowed for plume spreads in any of the three directions. The source strength was estimated by using the total loading of dust estimated by Iwasaka et al. (1983) and then distributing it uniformly over 4 day period, thus giving a value of 3.8E + 06 g/s.

The concentration at the observation site in Nagoya (longitude 137° E, latitude 35° N) was calculated to be in range of 100 to 300 $\mu g/m^3$. The estimated value was of the order of 600 $\mu g/m^3$ by Iwasaka et al. (1983). The calculated concentrations are lower, since the source was assumed to be continuous for 4 days, whereas in reality the dust is lifted into the air during frontal movements over the desert. Thus the duration of the emissions could be a short as a few hours. This gives greater dilution of the plume at the receptor region as compared to the real situation. The particle concentration was also calculated for the puff release case and these results are shown in Fig. 18. The calculated concentration for this case is in better agreement with the observed value. The source strength was unchanged in this run and the whole mass was released at the same moment. The predicted values are now greater than the estimated values. Thus, in reality, the source emissions appear to be of longer duration than a few hours. However, more precise information on the duration of the dust storm is not available.

6. Conclusions

Particle trajectories for dust in the Pacific Rim region were made using the conditioned particle method. Meteorological data, including the boundary layer turbulence statistics, were derived from a series of one-dimensional simulations of the atmospheric boundary layer using a K–E model. The locations for one-dimensional simulations were chosen to reflect the land/sea/land type of arrangement existing in this region. The K–E model with the algebraic stress component was shown to reproduce the major features of the boundary layer dynamics. The computed particle trajectories by this method are in agreement with those calculated by Iwasaka et al. (1983) using back trajectory computations from observed meteorological data. The plume widths were observed to grow continually over land surface. However, the plume did not grow appreciably after 48 h of diffusion time and while over the sea. The cause for this may be reduced shear and the strength of the diurnal oscillations. This point bears to be studied in further detail. Concentration profiles generated were in reasonable agreement with observed values.

In all the calculations performed the sedimentation of particles was neglected. For particles in the 0.1 to 1 μm range the particle settling velocities due to gravitation alone are in the range of 0.03 to 0.02 cm s^{-1}. With the centeroid of the plume at about 600 m, the effect of gravitational settling on particles of these sizes should be negligible. Larger particles will have much higher settling velocities and will be significantly effected. The particle size distribution reported by Iwasaka et al. (1983) is in the range of 0.3 to 10 μm and would probably settle to the ground by sticking to surfaces. In this respect the assumption of an elastic surface for particle impingement is questionable and the expected concentrations will be lower near the surface than those calculated here. But at points away from the surface the calculated concentrations should not be significantly effected.

The methodology described appears to be well suited for the study of regional scale transport and predicts some of the important behavioral patterns of these dust plumes. The results show that the inability to reproduce the turbulent statistics over the land sea interface may not be critical, in that the turbulence does not play a very important role after the first few hours in dispersing the plume. Further, the proper representation of boundary layer shear may be very critical in this type of computations and investigated further.

7. Acknowledgments

We thank Professor Ueda for his interest and guidance in completing the project. This work was supported in part by NASA grant #NAGW-2428. Computing resources were provided by IBM. The suggestions of the anonymous reviewers and the editor of the journal helped a great deal in improving the presentation of the results and are gratefully acknowledged.

REFERENCES

Andre, J. C., DeMoor, G., Lacarrere, P., Therry, G. and DuVachat, R. 1978. Modeling of the 24-hour evolution of the mean and turbulent structure of the planetary boundary layer. *J. Atmos. Sci.* **35**, 1861–1883.

Bhumralkar, C. M. 1975. Numerical experiments on the computation of ground surface temperature in an atmospheric general circulation model. *J. Appl. Meteor.* **14**, 1246–1258.

Bigg, E. K., Ayers, G. P. and Turvey, D. E. 1978. Measurements of the dispersion of a smoke plume at large distances from a source. *Atmos. Environ.* **12**, 1815–1818.

Carras, J. N. and Williams, D. J. 1981. The long range dispersion of a plume from an isolated point source. *Atmos. Environ.* **15**, 2205–2217.

Clarke, R. H. 1970. Recommended methods for the treatment of the boundary layer in numerical models. *Aust. Meteor.* **18**, 51–73.

Deardorff, J. W. 1974. Three dimensional numerical study of the height and mean structure of the heated planetary boundary layer. *Boundary layer Meteorology* **7**, 81–106.

Deardorff, J. W. 1978. Efficient prediction of ground surface temperature and moisture, with inclusion of a layer of vegetation. *J. Geophys. Res.* **83**, 1889–1903.

Duynkerke, P. G. 1988. Application of the E – e turbulence closure model to the neutral & stable atmospheric boundary layer. *J. Atmos. Sci.* **45**, 865–880.

GESAMP. 1989. The atmospheric input of trace species to the world oceans. *WMO Report #38.*

Gibbson, M. M. and Launder, B. E. 1978. Ground effects on pressure fluctuations in the atmospheric boundary layer. *J. Fluid Mech.* **86**, 491–511.

Gifford, F. A. 1982. Horizontal diffusion in the atmosphere: A Lagrangian-Dynamical theory. *Atmos. Environ.* **16**, 505–512.

Goodin, W. R., McRae, G. J. and Seinfeld, J. H. 1980. An objective analysis technique for constructing three dimensional urban-scale wind fields. *J. Appl. Meteor.* **19**, 98–108.

Hameed, S. and Dignon, J. 1988. Changes in the geographic distribution of global emissions of NO_x and SO_x from fossil fuel combustion between 1966 and 1980. *Atmos. Environ.* **22**, 3599–3617.

Hanna, S. A. 1981. Lagrangian and Eulerian time scale relations in the daytime boundary layer. *J. Appl. Meteor.* **20**, 242–249.

Iwasaka, Y., Minoura, K. and Nagoya, K. 1983. The transport and spatial scale of Asian dust-storm clouds: A case study of the dust-storm event of April 1979. *Tellus* **35B**, 189–196.

Kai, K., Okada, Y., Uchino, O., Tabata, I., Nakamura, H., Takasugi, T. and Nikaidou, Y. 1988. Lidar observations and numerical simulation of a KOSA (Asian Dust) over Tsukuba, Japan, during the spring of 1986. *J. Meteor. Soc. Japan* **66**, 457–472.

Kitada, T. 1987. Turbulence structure of sea breeze front and its implications in air pollution transport-application of $K-\varepsilon$ turbulence model. *Boundary Layer Meteorology* **41**, 217–239.

Kondo, Y., Mathews, W., Iwata, A., Morita, Y. and Takagi, M. 1987. Aircraft measurements of Oxides of Nitrogen along the eastern rim of the Asian continent: Winter observations. *J. Atmos. Chem.* **5**, 37–58.

Kotamarthi, V. R. and Carmichael, G. R. 1990. The long range transport of pollutants in the Pacific rim region. *Atmos. Environ.* **24A**, 1521–1534.

Legg, B. J. and Raupach, M. R. 1982. Markov chain simulation of particle dispersion in inhomogeneous flows: the mean drift velocity induced by a gradient in Eulerian velocity variance. *Boundary Layer Meteorology* **24**, 3–13.

Ley, A. J. 1982. A random walk simulation of two-dimensional turbulent diffusion in the neutral surface layer. *Atmos. Environ.* **16**, 2799–2808.

McNider, R. T., Moran, M. D. and Pielke, R. A. 1988. Influence of diurnal and inertial boundary layer oscillation on long-range dispersion. *Atmos. Environ.* **22**, 2445–2462.

Mellor, G. L. and Yamada, T. 1974. A hierarchy of turbulence closure models for planetary boundary layer. *J. Atmos. Sci.* **31**, 1791–1806.

Merrill, J. T., Bleck, R. and Avila, L. 1985. Modeling atmospheric transport to the Marshall Islands. *J. Geophys. Res.* **90**, D7, 129297–12936.

O'Brien, J. J. 1970. A Note on the vertical structure of the eddy exchange coefficient in the planetary boundary layer. *J. Atmos. Sci.* **27**, 1213–1215.

Pasquill, F. and Smith, F. B. 1983. *Atmospheric diffusion.* Ellis Horwood Limited, 437 pp.

Pielke, R. A. 1984. *Mesoscale meteorological modeling.* Academic Press, 612 pp.

Pielke, R. A. and Mahrer, Y. 1975. Representation of the heated planetary boundary layer in mesoscale models with coarse vertical resolution. *J. Atmos. Sci.* **32**, 2288–2308.

Prospero, J. M. and Savoie, D. L. 1989. Effect of continental sources on nitrate concentration over the Pacific Ocean. *Nature* **339**, 687–689.

Reid, J. D. 1979. Markov chain simulations of vertical dispersion in the neutral surface layer for surface and elevated releases. *Boundary Layer Meteorology* **16**, 3–22.

Richtmyer, R. D. and Morton, K. W. 1967. *Difference methods for initial-value problems.* Inter Science, 405 pp.

Rodi, W. 1976. A new algebraic relation for calculating the reynolds stresses. *ZAMM 56*, T219–T211.

Rodi, W. 1985. Calculation of stably stratified shear-layer flows with a buoyancy-extended $\kappa-\varepsilon$ turbulence model. *Turbulence and diffusion in stable environments* (ed. J. C. R. Hunt). Oxford Univ. Press, 319 pp.

Sasamori, T. 1968. The radiative cooling calculation for application to general circulation experiments. *J. Applied Meteor.* **7**, 721–729.

Smith, F. B. 1968. Conditioned particle motion in a homogeneous turbulent field. *Atmos. Environ.* **2**, 491–508.

Stubley, G. D. and Rooney, D. R. 1986. The sensitivity of $k-e$ model computation of the neutral planetary boundary layer to Baroclinicity. *Boundary layer Meteorology* **37**, 53–70.

Sun, W. Y. and Chang, C. Z. 1986. Diffusion model for a convective layer. Part 1. Numerical simulation of convective boundary layer. *J. Climate Appl. Meteor.* **25**, 1445–1453.

Suzuki, T. and Tsunogai, S. 1988. Daily variation of aerosol of marine and continental origin in the surface air over a small Island, Okushiri, in the Japan Sea. *Tellus* **40B**, 42–49.

Thomson, D. J. 1984. Random walk modeling of diffusion in homogeneous turbulence. *Quart. J. R. Met. Soc.* **110**, 1107–1120.

Uno, I. and Ueda, H. 1988. Some contributions to the algebraic stress turbulence model to the application of stratified flows. *Proceeding of the 3rd International Symposium on Refined flow modeling of turbulence measurements*, Tokyo, 26–28 July, 1988.

Uno, I., Ueda, H. and Wakamatsu, S. 1989. Numerical modeling of the nocturnal urban boundary layer. *Boundary Layer Meteorology* **49**, 77–98.

Yamada, T. and Bunker, S. 1988. Development of a nested grid, second moment turbulence closure model and application to the 1982 ASCOT Brush Creek data simulation. *J. Appl. Meteor.* **27**, 562–578.

Yamada, T. and Mellor, G. 1975. A simulation of the Wangara atmospheric boundary layer data. *J. Atmos. Sci.* **32**, 2309–2329.

Tellus B/45/5-4